

Correlation and Covariance of Satellite Scatterometer Measurements

Peter K. Yoho, *Member, IEEE*, and David G. Long, *Senior Member, IEEE*

Abstract—Recently, more capable scatterometer designs have been developed that seek improved resolution through the use of higher pulse sampling rates. The high sampling rates bring the traditional scatterometry assumption of measurement independence into question. This paper uses fundamental scattering theory to derive general expressions for correlation and covariance between scatterometer measurements and provides practical analysis using current and future instruments as examples. The paper derives expressions for the measurement variance parameter K_p when measurement correlation due to Rayleigh fading effects is present and relates K_p to the statistics of multiple pulse measurements. A function of the transmit signal modulation and receive processing, the measurement correlation is zero for nonoverlapping measurements but can become significant for overlapping measurements at high pulse sampling rates. The paper discusses the effects of correlation on the accuracy of scatterometer measurements and evaluates tradeoffs between spatial overlap, levels of additive noise, and measurement precision.

Index Terms—Correlation, covariance, Hydrosphere States Mission (HYDROS), K_p , QuikSCAT, scatterometry, SeaWinds.

I. INTRODUCTION

SATELLITE scatterometers have demonstrated an ability to not only estimate ocean wind speed and direction, their original goal, but to also investigate sea ice extent, iceberg location, snow melt cycles, and tropical deforestation [1]. The emergence of additional applications has become a catalyst for development of more capable instruments and new data processing algorithms. New algorithms exploit the spatial overlap and dissimilar geometry of colocated measurements, for new and old instruments alike, to improve the effective measurement resolution [2]. New scatterometer designs seek to increase resolution by providing more surface samples and processing the signal response more effectively [3].

The designs of newer instruments provide dense, overlapping samples of the surface, a significant change from earlier instruments. This introduces several issues that have not been explored in detail previously. A key issue addressed here is correlation between individual measurements. When measurements overlap, correlation in Rayleigh signal fading decreases the number of independent samples, degrading data accuracy and precision. The precise degradation is a function

of the transmit signal modulation, receive processing, pulse rate, and antenna gain pattern.

This paper mathematically derives expressions for the correlation of scatterometer measurements and discusses its effect on measurement accuracy. The paper is organized as follows. Section II presents principles relevant to the discussion of scatterometer measurements, such as scattering and fading and develops a general signal measurement model. It then derives expressions for multimeasurement statistics. Section III considers additive noise. The full theory statistically accounts for the combined random fluctuations of additive thermal noise and multiplicative signal fading. Section IV provides analysis of derived coefficients, focusing on a covariance term present in the correlation and covariance expressions. The section applies the derived results to two pencil-beam instruments to provide general guidelines of how the measurement process effects correlation values. Section V then uses the results of Sections II and III to define the commonly used metric K_p for multiple pulse measurements. It discusses the effects of correlation on K_p as well as tradeoffs that exist between pulse correlation, noise power, and measurement precision. Finally, Section VI summarizes findings and concludes.

II. INTERACTION AND STATISTICS OF MULTIPLE MEASUREMENTS

Traditionally, consecutive measurements from satellite scatterometers have been assumed to be independent. This assumption is based on the short correlation length of natural surfaces and minimal spatial overlap between measurements. Newly proposed systems that oversample the surface require reconsideration of this assumption. While the spacing between measurements for these instruments is more than the correlation length of the surface, it is not large enough to justify independence of fading between pulses, since the measurement footprints significantly overlap. In such cases, the signal fading may be correlated between pulses. We, thus, consider the relationship between multiple measurements starting with first principles.

A. Surface Scattering for Distributed Targets

When a microwave radar signal impacts the surface a portion of the signal, energy is reflected back toward the origin of the incident wave; this reflection is termed backscatter and can be represented for a point target by the complex value z , the voltage electric field of the backscatter. The large footprint area of scatterometer measurements causes the transmitted signal to be simultaneously incident on a large number of scatterers, termed a distributed area target. The response from a distributed target

Manuscript received August 19, 2003; revised January 7, 2004. This work was supported by the Jet Propulsion Laboratory, National Aeronautics and Space Administration.

P. K. Yoho is with the Lincoln Laboratory, Massachusetts Institute of Technology, Lexington, MA 02420 USA (e-mail: yoho@ll.mit.edu).

D. G. Long is with the Department of Electrical and Computer Engineering, Brigham Young University, Provo, UT 84602 USA (e-mail: long@ee.byu.edu).
Digital Object Identifier 10.1109/TGRS.2004.825588

can be modeled by the coherent sum of the response from each point scatterer

$$Z = \sum_i z_i = v_d e^{j\phi_d} \quad (1)$$

with magnitude v_d , which is Rayleigh distributed, and phase ϕ_d , which is uniformly distributed [4]. Applying the central limit theorem (by assuming that there are a large number of scatterers in the distributed response) and assuming that no scatterer dominates the overall return, the real and imaginary parts of the individual responses r_i and q_i may be assumed to be independent normally distributed random variables with mean zero and variance σ [4]. The expected value of the voltage magnitude is $\mathcal{E}[v_d] = \sqrt{\pi/2}\sigma$, where \mathcal{E} is the expected value operator; the second moment of the voltage magnitude is $\mathcal{E}[v_d^2] = 2\sigma^2$. We assume that v_d and ϕ_d are independent for each distributed target considered. This is reasonable considering that most surface features have submeter correlation lengths, and most scatterometer measurements encompass several kilometers. We also assume stationarity for both magnitude and phase of the distributed targets. The normalized radar cross section of the area σ° is related to the voltage response by

$$\mathcal{E}[v_d^2] = \mathcal{E}[|Z|^2] = A_d \sigma^\circ \quad (2)$$

where A_d is the area of the distributed target. σ° is, therefore, proportional to the variance of real and imaginary parts of the individual scatterers.

Using the properties of a uniform distribution, the correlation between the response of two distributed targets can be written as

$$\mathcal{E}[Z(a)Z^*(b)] = A_d(a)\sigma_d^\circ(a)\delta(a-b). \quad (3)$$

Later, it will also be necessary to utilize the fourth-order expectation of distributed targets, which can be shown to be

$$\begin{aligned} \mathcal{E}[Z(a)Z^*(b)Z(c)Z^*(d)] &= A_d(a)\sigma^\circ(a)\delta(a-b)A_d(c)\sigma^\circ(c) \\ &\quad \cdot \delta(c-d) + A_d(a)\sigma^\circ(a)\delta(a-d) \\ &\quad \cdot A_d(c)\sigma^\circ(c)\delta(b-c). \end{aligned} \quad (4)$$

B. Scatterometer Signals

A scatterometer transmits a modulated carrier signal of the form (for convenience complex signals are assumed)

$$\xi_t(t) = \sqrt{E_t} a(t) e^{j\omega_c t} \quad (5)$$

where t is time, E_t is the total transmitted energy for a single pulse, ω_c is the angular center frequency, and $a(t)$ is the complex modulation function with

$$\int_0^{T_a} |a(t)|^2 dt = 1 \quad (6)$$

and $a(t) = 0$ for $t < 0$ and $t > T_a$.

Ignoring spreading loss and antenna gain for the moment, the echo return of the scatterometer signal from a single point scatterer can be written as

$$\xi_r(t) = z \left(\sqrt{E_t} a \left(t - \frac{2r}{c} \right) e^{j\omega_c t} e^{-j\omega_d t} e^{\frac{j2\omega_c r}{c}} \right) \quad (7)$$

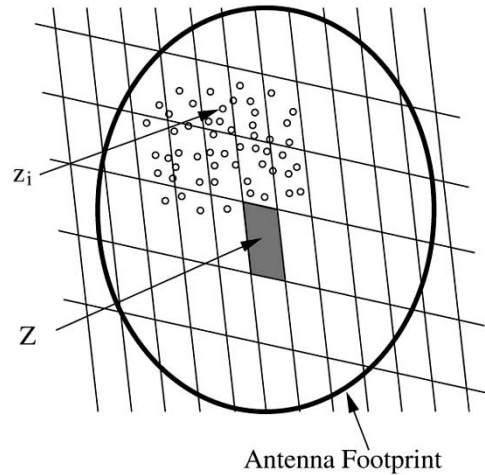


Fig. 1. Simplified geometry of a scatterometer footprint. Each z_i represents an individual scatterer. Z is the total voltage response of one resolution element, consisting of a large number of individual scatterers. The elliptical footprint is the 3-dB contour of the illumination pattern.

where r is the range from instrument to the point scatterer, and ω_d is the Doppler shift of the point. This expression assumes that changes in spacecraft velocity during the transmission and reception cycle need not be considered in the Doppler shift, which generally holds when pulse periods are less than 1 s and center frequencies are greater than 1 GHz [5]. Accounting for antenna gain and spreading loss terms, the return signal echo for the i th scatterer can be written as

$$\begin{aligned} \xi_r(t, i) &= z_i \left(\frac{G(i)\lambda}{(4\pi)^{\frac{3}{2}} r^2(i)} \right) \\ &\quad \cdot \left(\sqrt{E_t} a \left(t - \frac{2r(i)}{c} \right) e^{j\omega_c t} e^{-j\omega_d(i)t} e^{\frac{j2\omega_c r(i)}{c}} \right) \end{aligned} \quad (8)$$

where λ is the signal's wavelength, and G is the antenna gain in the direction of the point scatterer.

C. Instrument Measurement

Without some form of Doppler or range filtering, the resolution of a measurement is limited to the size of the antenna footprint, typically described by the antenna pattern 3-dB beam width. Utilizing Doppler and/or range filtering improves the effective resolution of the instrument by separating the antenna footprint into multiple distributed targets [3]. Fig. 1 illustrates this principle for a general footprint geometry. The large ellipse represents an antenna footprint and the straight lines represent an arbitrary resolution grid generated by range and Doppler filtering. The maximum resolution of a scatterometer is a function of pulse length, signal wavelength, frequency modulation, and processing, and constitutes a single resolution element. For scatterometers, this limit is generally on the order of hundreds of meters, allowing us to assume that a large number of scatterers exist in every resolution element and, thus, enabling us to apply the properties of distributed targets.

Using (1) the return echo from each resolution element consists of the sum of the individual point scatterers within the element

$$\xi_r(t, n) = \frac{\sqrt{E_t}\lambda}{(4\pi)^{\frac{3}{2}}} \sum_{i_n} z_{i_n} G(i_n) a \left(t - \frac{2r(i_n)}{c} \right) \frac{e^{j\omega_c t} e^{-j\omega_d(i_n)t} e^{\frac{j2\omega_c r(i_n)}{c}}}{r^2(i_n)} \quad (9)$$

where the sum is over the i scatterers within the n th resolution element. For a satellite, the range term is very large in comparison to the change in range for each element. We, therefore, assume that the denominator r^2 is constant over the sum for each resolution element and use its mean value \bar{r}^2 . For simplicity, we also assume that gain and observed Doppler are constant over each resolution element, and that the group time delay and phase shift can be sufficiently modeled using the mean range value for each resolution element. Employing an orthogonal (x, y) coordinate system aligned with the along-track and cross-track directions of the spacecraft, the return signal for each element is

$$\xi_r(t, x, y) = \frac{\sqrt{E_t}\lambda}{(4\pi)^{\frac{3}{2}}\bar{r}^2} Z(x, y) G(x, y) a \left(t - \frac{2\bar{r}(x, y)}{c} \right) \cdot e^{j\omega_c t} e^{-j\omega_d(x, y)t} e^{\frac{j2\omega_c \bar{r}(x, y)}{c}} \quad (10)$$

which is the generalized return signal for a scatterometer.

Scatterometers make measurements of distributed targets in a variety of ways, depending upon requirements for resolution, the instrument modulation function, receiver hardware, and signal processing. In general, instruments use a form of square-law detection, allowing the measurements to be written as

$$M^s = \Omega |\Omega \xi_r(t, x, y)|^2 \quad (11)$$

where M^s denotes a signal measurement and the Ω operator represents summation, either discrete or continuous, over area and/or time, as required to describe the resolution filtering used by a specific instrument. A low-resolution measurement utilizing square-law detection and no filtering can be described by

$$M^{\text{as}} = \int_t \left| \int_x \int_y \xi_r(t, x, y) dy dx \right|^2 dt \quad (12)$$

the superscript in M^{as} denoting antenna resolution, t spans the duration of the return echo, and x and y span the footprint area. Filtering with maximal resolution over range and Doppler can be modeled as

$$M^{\text{ms}} = \left| \int_{\omega} \int_t \int_x \int_y F(t, \omega) \xi_r(t, x, y) dy dx dt d\omega \right|^2 \quad (13)$$

where $F(t, \omega)$ represents the resolution filtering process in time (t) and frequency (ω) and consists of a linear operator, usually convolution with a matched filter. Recent pencil-beam scat-

terometers have adopted a one-dimensional (1-D) range filtering scheme, which can be modeled as

$$M^{\text{fs}} = \int_{\omega} \left| \int_t \int_x \int_y F(t, \omega) \xi_r(t, x, y) dy dx dt \right|^2 d\omega \quad (14)$$

the superscript in M^{fs} denoting a filtered signal measurement.

D. Measurement Statistics

The general statistical properties of a scatterometer measurement have been calculated for several different instruments and measurement configurations [5]–[7]. These studies derived the statistics of single independent measurements using various measurement forms. It is our desire to extend the theory by considering multiple spatially overlapping measurements and the correlation between them.

For convenience, we define the radar calibration parameter X as

$$X = \frac{E_t \lambda^2 G_o^2 A_E}{(4\pi)^3 \bar{r}^4} \quad (15)$$

with G_o as the peak antenna gain and A_E as the effective measurement area

$$A_E = \frac{1}{G_o^2} \int_x \int_y G^2(x, y) A_d(x, y) dy dx. \quad (16)$$

We also define the receive signal term Y as

$$Y(t, x, y) = \frac{1}{G_o \sqrt{A_E}} G(x, y) a \left(t - \frac{2\bar{r}(x, y)}{c} \right) \cdot e^{j\omega_c t} e^{-j\omega_d(x, y)t} e^{\frac{j2\omega_c \bar{r}(x, y)}{c}} \quad (17)$$

so that the noise-free receive signal from each resolution element can be written as

$$\xi_r(t, x, y) = \sqrt{XY}(t, x, y) Z(x, y). \quad (18)$$

To aid understanding of how the measurement form employed affects the values of signal correlation and covariance, as well as to demonstrate a generalized result, we develop expressions for both the antenna footprint resolution case (12) and the 1-D filtering case (14). The process can be easily expanded to the full-resolution case (13) as desired.

For (12), the expected value of an antenna footprint resolution signal measurement M^{as} is

$$\mathcal{E}[M^{\text{as}}] = \mathcal{E} \left[\int_t \left| \int_x \int_y \xi_r(t, x, y) dy dx \right|^2 dt \right] = X R^a \quad (19)$$

where R^a is

$$R^a = \int_t \int_x \int_y |Y(t, x, y)|^2 A_d(x, y) \sigma^o(x, y) dy dx dt. \quad (20)$$

The correlation of two measurements M_k^{as} and M_l^{as} can then be shown to be

$$\mathcal{E}[M_k^{\text{as}} M_l^{\text{as}}] = X_k X_l [R_k^a R_l^a + V_{kl}^a] \quad (21)$$

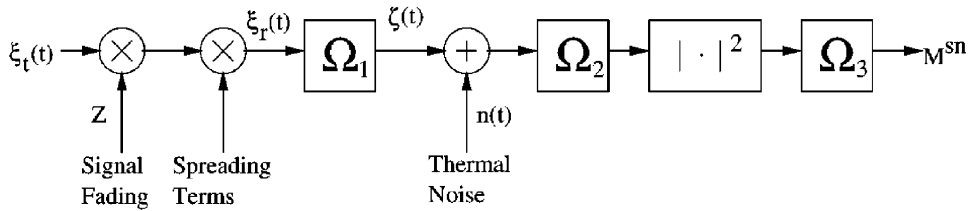


Fig. 2. Generalized signal flowgraph of a scatterometer measurement. The flowgraph models the measurement process for backscatter, incorporating additive noise and signal processing to generate the measurement. The Ω operators are defined in the text.

with

$$V_{kl}^a = \int_{t_k} \int_{t_l} \int_{x_k} \int_{x_l} \int_{y_k} \int_{y_l} \int \sigma^\circ(x_k, y_k) \sigma^\circ(x_l, y_l) A_d(x_k, y_k) \cdot A_d(x_l, y_l) Y(t_k, x_k, y_k) Y^*(t_k, x_l, y_l) Y(t_l, x_l, y_l) \cdot Y^*(t_l, x_k, y_k) dy_l dx_l dy_k dx_k dt_l dt_k. \quad (22)$$

The covariance $\text{Cov}[M_k^{\text{as}} M_l^{\text{as}}]$ of two measurements can also be shown to be

$$\text{Cov}[M_k^{\text{as}} M_l^{\text{as}}] = X_k X_l V_{kl}^a. \quad (23)$$

Similarly, for the 1-D filtering measurement case (14) the expected value of the signal is

$$\mathcal{E}[M^{\text{fs}}] = \mathcal{E} \left[\int_{\omega} \left| \int_t \int_x \int_y F(t, \omega) \xi_r(t, x, y) dy dx dt \right|^2 d\omega \right] = X R^f \quad (24)$$

where R^f is

$$R^f = \int_{\omega} \int_t \int_{t'} \int_x \int_y A_d(x, y) \sigma^\circ(x, y) F(t, \omega) F^*(t', \omega) \cdot Y(t, x, y) Y^*(t', x, y) dy dx dt' dt d\omega. \quad (25)$$

The correlation of two measurements M_k^{fs} and M_l^{fs} is then

$$\mathcal{E}[M_k^{\text{fs}} M_l^{\text{fs}}] = X_k X_l [R_k^f R_l^f + V_{kl}^f] \quad (26)$$

where V^f is

$$V_{kl}^f = \int_{\omega_k} \int_{\omega_l} \int_{t_k} \int_{t'_k} \int_{t_l} \int_{t'_l} \int_{x_k} \int_{x_l} \int_{y_k} \int_{y_l} A_d(x_k, y_k) A_d(x_l, y_l) \cdot \sigma^\circ(x_k, y_k) \sigma^\circ(x_l, y_l) F(t_k, \omega_k) F^*(t'_k, \omega_k) F(t_l, \omega_l) \cdot F^*(t'_l, \omega_l) Y(t_k, x_k, y_k) Y^*(t'_k, x_l, y_l) Y(t_l, x_l, y_l) \cdot Y^*(t'_l, x_k, y_k) \cdot dy_l dy_k dx_l dx_k dt'_l dt'_k dt'_k d\omega_l d\omega_k. \quad (27)$$

The covariance of two measurements is

$$\text{Cov}[M_k^{\text{fs}} M_l^{\text{fs}}] = X_k X_l V_{kl}^f. \quad (28)$$

We can also frequently assume that σ° is constant over the measurement area. When true, we can define alternate forms of R^a , V^a , R^f , and V^f using a bar, i.e., $R^a = \sigma^\circ \bar{R}^a$, to signify such independence.

The expressions in (21), (23), (26), and (28) are the results we desire. When $k = l$, the correlation for both (21) and (26) simplifies to the second moment

$$\mathcal{E}[(M^s)^2] = X^2[R^2 + V] \quad (29)$$

where R represents either R^a or R^f as appropriate, and the covariance equals the variance of the measurement $X^2 V$ (V^a or V^f). In the case of antenna footprint resolution, the values for the second moment and variance are identical to those shown by Long and Spencer [5]. If $k = l$ and M_k^s and M_l^s (M^{as} or M^{fs}) are completely independent, V is zero, the covariance is subsequently zero, and the correlation simplifies to the square of the expected value $\mathcal{E}^2[M^s] = (XR)^2$ for both measurement forms.

The derivation of correlation and covariance expressions for two versions of scatterometer measurements (12) and (14) demonstrate the effect that various configurations have on the statistical expressions. The two versions can be made equivalent by choosing $F(t, \omega) = \delta(t - \omega)$ in (14) so that $V^f = V^a$. This allows us to conclude that the filtered form of instrument measurements (14) is sufficiently general to emulate most measurement configurations and, thus, is used throughout the remainder of the paper.

III. NOISY SIGNAL MEASUREMENTS

The next step in our analysis is to consider random fluctuations caused by sources other than the surface. Consider the general measurement model shown in Fig. 2, where multiplicative signal fading has already been considered. The output of the first Ω operator Ω_1 for our model is

$$\zeta(t) = \int_x \int_y \xi_r(t, x, y) dy dx. \quad (30)$$

The second random term in the model is additive noise $n(t)$, which results from radiometric and thermal noise. The total system noise is traditionally measured in terms of brightness temperature T_{sys} and is a linear combination of T'_A , the radiometric antenna temperature, and T'_{rec} , the receiver noise temperature independent of the received radiation [8]

$$T_{\text{sys}} = T'_A + T'_{\text{rec}}. \quad (31)$$

Both terms are random variables and are assumed to have Gaussian distributions. For scatterometers, T'_{rec} is significantly larger than T'_A and dominates the noise term. Thus, for our derivation, the overall thermal noise term $n(t)$ is placed as shown in Fig. 2.

To assess the effects of noise on surface measurements, we define the statistical properties of the noise. First, since the receiver noise dominates, we assume that the additive thermal noise $n(t)$ is a real zero-mean Gaussian process, independent of the received signal $\zeta(t)$, so that $\mathcal{E}[\zeta(t)n(t)] = \mathcal{E}[\zeta(t)]\mathcal{E}[n(t)] = 0$. Second, we assume that the instrument receiver measures the signal and noise over a finite bandwidth B_r . We assume that B_r

is larger than the signal bandwidth and that the filters used to constrain the bandwidth are ideal. The filtered noise-only signal $\nu(t)$ is

$$\nu(t) = h(t) * n(t) \quad (32)$$

where $h(t)$ is the impulse response of the bandlimiting filter.

The noise-only signal $n(t)$ is assumed to have a power spectral density of $n_o/2$ over the measurement bandwidth so that the correlation of the filtered noise is $\mathcal{E}[\nu(t)\nu^*(t - \tau)] = 2B_r(n_o/2)\text{sinc}(2B_r[t - \tau])$ where the filter response is an ideal lowpass filter. For the 1-D measurement filtering case (14), the expected value of a noise-only measurement is

$$\mathcal{E}[M^n] = \mathcal{E} \left[\int_{\omega} \left| \int_t F(t, \omega) \nu(t) dt \right|^2 d\omega \right] \quad (33)$$

$$= \int_{\omega} \int_t \int_{t'} F(t, \omega) F^*(t', \omega) 2B_r \left(\frac{n_o}{2} \right) \cdot \text{sinc}(2B_r[t - t']) dt' dt d\omega \quad (34)$$

$$= \mathcal{N}_s. \quad (35)$$

Using these definitions, the signal-plus-noise measurement M^{sn} is expressed as

$$M^{\text{sn}} = \int_{\omega} \left| \int_t F(t, \omega) [h(t) * (\zeta(t) + n(t))] dt \right|^2 d\omega \quad (36)$$

$$= \int_{\omega} \left| \int_t F(t, \omega) [\zeta(t) + \nu(t)] dt \right|^2 d\omega \quad (37)$$

with expected value

$$\mathcal{E}[M^{\text{sn}}] = XR^f + \mathcal{N}_s. \quad (38)$$

We can then show that the correlation of two noisy measurements M_k^{sn} and M_l^{sn} is

$$\begin{aligned} \mathcal{E}[M_k^{\text{sn}} M_l^{\text{sn}}] &= X_k X_l \left[R_k^f R_l^f + V_{kl}^f \right] + X_k R_k^f \mathcal{N}_s \\ &+ X_l R_l^f \mathcal{N}_s + \mathcal{N}_s^2 + \delta(k - l) (2XR^f \mathcal{N}_s + 2\mathcal{N}_s^2) \end{aligned} \quad (39)$$

and the covariance of the measurements is

$$\text{Cov}[M_k^{\text{sn}} M_l^{\text{sn}}] = X_k X_l V_{kl}^f + \delta(k - l) (2XR^f \mathcal{N}_s + 2\mathcal{N}_s^2). \quad (40)$$

Results are similar for other measurement forms.

The results for the noisy correlation and covariance are similar to those found in the noise free case (26) and (28). In particular, since noise is assumed to be independent, the covariance of the noisy and noise free cases is identical for $k \neq l$. If the measurements are the same ($k = l$), then the covariance contains additional terms that account for the added variance due to noise.

Scatterometers remove the noise-induced bias in the signal plus noise expectation (38) by subtracting a separate noise-only measurement M^n from the noisy signal measurement. This noise-only measurement is made either by expanding the primary measurement bandwidth and estimating the noise from spectral areas where the signal is not present, or by making

a noise-only measurement at a different time than the receive echo signal. The expected value of the noise-only measurement is defined as $\mathcal{E}[M^n] = \mathcal{N}_n$.

The unbiased measurement of the signal M^u is

$$M^u = \alpha M^{\text{sn}} + \beta M^n \quad (41)$$

where α and β are appropriately chosen so that $\mathcal{E}[M^u] = X\sigma^o$, which makes the measurement unbiased to noise, i.e.,

$$\alpha = (\bar{R})^{-1} \quad \beta = -\frac{\mathcal{N}_s}{\bar{R}\mathcal{N}_n} \quad (42)$$

for all measurement forms.

To determine the correlation and covariance of the unbiased noisy measurement form, we first define the correlation between the noisy measurement and the noise-only measurement as

$$\mathcal{E}[M^{\text{sn}} M^n] = XR\mathcal{N}_n + \mathcal{N}_s \mathcal{N}_n \quad (43)$$

and the correlation of two noise-only measurements as

$$\mathcal{E}[M_k^n M_l^n] = \mathcal{N}_n^2 + \delta(k - l) 2\mathcal{N}_n^2. \quad (44)$$

We can then show the correlation of two unbiased measurements to be

$$\mathcal{E}[M_k^u M_l^u] = \frac{X_k X_l}{\bar{R}_k \bar{R}_l} \left(R_k R_l + V_{kl} + \delta(k - l) \left[\frac{2R\mathcal{N}_s}{X} + \frac{4\mathcal{N}_s^2}{X^2} \right] \right) \quad (45)$$

and the covariance of an unbiased noisy measurement to be

$$\text{Cov}[M_k^u, M_l^u] = \frac{X_k X_l}{\bar{R}_k \bar{R}_l} \left(V_{kl} + \delta(k - l) \left[\frac{2R\mathcal{N}_s}{X} + \frac{4\mathcal{N}_s^2}{X^2} \right] \right). \quad (46)$$

These results highlight the fact that additive noise affects only the autocorrelation and autocovariance (variance) statistics of a measurement regardless of measurement form. For distinct measurements ($k \neq l$), the noise is uncorrelated from both the signal and from pulse to pulse. In this case, the measurement correlation and covariance depend only upon the random fluctuations of the measured surface and not upon any noise-induced variation. We note that when the measurement gain patterns do not overlap the covariance of the measurements is zero. The covariance is nonzero when the patterns overlap and depends on the modulation and receive processing.

IV. ANALYSIS OF THE SIGNAL COVARIANCE EXPRESSION

To better understand signal covariance, we analyze \bar{V} for two instruments, the SeaWinds scatterometer [7] and the proposed Hydrosphere States Mission (HYDROS) instrument [10]. Both instruments make measurements by conically scanning a pencil-beam antenna about nadir (see Fig. 3) and generally have the same footprint size of 36 km \times 26 km (SeaWinds' outer beam). Both instruments provide two data products: SeaWinds produces a footprint resolution measurement (12) and a range filtered measurement (14) [7]; HYDROS produces a high-resolution two-dimensional filtered product (13) and a low-resolution diagnostic product (12) [9].

The key difference of the two instruments is their pulse rate. While SeaWinds transmits 1.5 ms pulses every 10.8 ms, each having a bandwidth of 375 kHz, HYDROS transmits 15- μ s pulses every 286 μ s, each having a bandwidth of 1 MHz. SeaWinds' rotation rate and PRF locate consecutive pulses

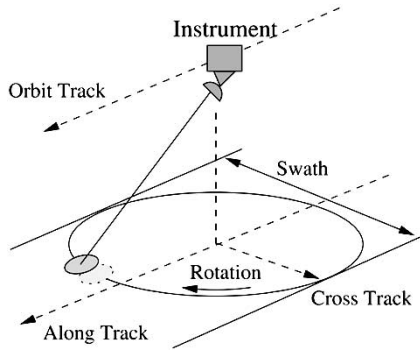


Fig. 3. Geometry of a conically scanning pencil-beam spaceborne scatterometer [7].

18 km apart in azimuth, which encourages the assumption of independence. HYDROS' rotation rate and PRF locate consecutive pulses 210 m apart in azimuth, bringing this assumption into question.

Both instruments use a linear frequency modulated (LFM), or chirped, pulse. We model this pulse as

$$a_k(t) = \frac{1}{\sqrt{T_a}} e^{j2\pi(\frac{1}{2})\mu t^2}, \quad 0 + kT_p \leq t \leq T_a + kT_p \quad (47)$$

where μ is the chirp rate, and T_p is the period of the pulse, or pulse repetition increment, and assume that each pulse is equivalent in shape and modulation.

A. Footprint Resolution (\bar{V}^a)

We first consider the term \bar{V}^a , which corresponds to the low-resolution antenna footprint measurements produced by SeaWinds and HYDROS. We show that by simplifying the expression we gain clarity and insight into causes of measurement covariance. We use the generalized radar ambiguity function [4]

$$\mathcal{X}(t, \omega) = \int_{-\infty}^{+\infty} a(y)a^*(y+t)e^{j\omega y} dy. \quad (48)$$

We note that $a(y)$ is zero outside the time limits of the pulse and assume that instrument range gates are sufficiently wide to admit all of the echo signal. This allows us to extend the time limits of \bar{V}^a to infinity without affecting the total value of the integral. Implementing these changes, \bar{V}^a can be written as

$$\bar{V}_{kl}^a = \int_{x_k} \int_{y_k} \int_{x_l} \int_{y_l} \mathcal{X}^2(d_r, f_\omega) Q(x_k, y_k) Q(x_l, y_l) \cdot B_{kl}(f_\omega) dy_l dx_l dy_k dx_k \quad (49)$$

where $d_r = (2/c)(r(x_l, y_l) - r(x_k, y_k))$ and $f_\omega = -[\omega_d(x_l, y_l) - \omega_d(x_k, y_k)]/2\pi$ represent a change of variables for the ambiguity function. The cross-pulse gain product is $Q(x_k, y_k) = A_d(x_k, y_k)G_k(x_k, y_k)G_l(x_k, y_k)$, and $B_{kl}(f_\omega)$ is the covariance phase expression defined as

$$B_{kl}(f_\omega) = e^{-jf_\omega T_p(t-k)}. \quad (50)$$

The characteristics of the radar ambiguity function are determined by the pulse modulation function $a(t)$. For an interrupted continuous wave pulse the ambiguity function has a triangular shape in the time dimension and a sinc-like shape in

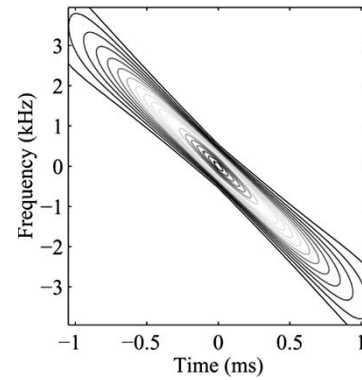


Fig. 4. Radar ambiguity function for a single LFM pulse with a down chirp.

the frequency dimension. The ambiguity function for a linear frequency modulated (LFM) pulse is often referred to as a "knife blade" due to its sharp diagonal peak. The major axis of the blade is sloped in the time-frequency plane, with the slope determined by the chirp rate. The width of the blade in the time dimension is determined by the duration of the pulse and the width of the response in the frequency direction is proportional to the reciprocal of the pulse repetition period (see Fig. 4).

The relatively high chirp rates for both SeaWinds and HYDROS cause the major axis of the razor blade to be almost vertical, HYDROS more so than SeaWinds, in the time-frequency plane, so that the ambiguity function is nominally invariant for small frequencies and a delta function in time.

The second term in (49), the cross-pulse gain product $Q(x, y)$, is a product of the antenna patterns of the two pulses multiplied by the differential measurement area. If the two pulses are identical ($k = l$), then $Q(x, y) = A_d(x, y)G^2(x, y)$; if they have no overlap, then $Q(x, y) = 0$. For most previous instruments, including SeaWinds, the large spacing between pulses reduces Q , minimizing \bar{V}^a and making measurement covariance nominally zero.

The third term in (49), the covariance phase B_{kl} , is also a major contributor to measurement correlation. This can be illustrated by assuming, for the moment, that $G(x, y)$ is an ideal footprint

$$G(x, y) = \begin{cases} 1, & -\frac{X}{2} \geq x \geq \frac{X}{2} \text{ and } -\frac{Y}{2} \geq y \geq \frac{Y}{2} \\ 0, & \text{else} \end{cases} \quad (51)$$

so that \bar{V}^a can be expressed as

$$\bar{V}_{kl}^a = \int_{-X}^X \int_{-Y}^Y (X - |r_d|)(Y - |f_\omega|) \Re \{B_{kl}(f_\omega)\} \cdot \mathcal{X}^2(r_d, f_\omega) dr_d df_\omega \quad (52)$$

where \Re references the real part of B_{kl} . We note that \bar{V}^a is always real and conforms with previously derived results for $k = l$ [5].

The covariance phase, or more precisely the real part of the phase, is a sinc function where B_d is the Doppler bandwidth of the return echo. If $B_d T_p \geq 1$, then $B_{kl} \approx \delta(k - l)$ and each measurement is independent. This is the case for SeaWinds. For HYDROS at 90° azimuth, $B_d T_p \approx 0.55$. This translates to a correlation value of 30% for consecutive pulses. Results for other values of $l - k$ at 90° are shown in Fig. 5.

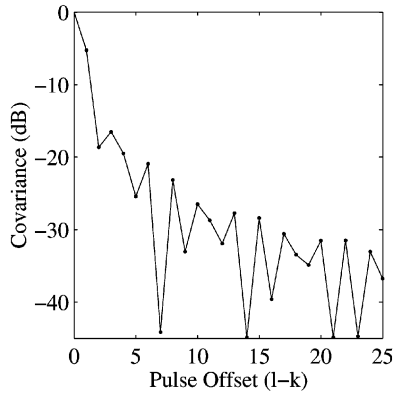


Fig. 5. Plot of \bar{V}_{kl}^a at 90° azimuth as a function of $l - k$ for the HYDROS instrument. The figure shows that consecutive pulses have a covariance of 0.30, and pulses offset by more than two pulses are essentially independent.

Using $B_{kl}(f_\omega)$ the level of pulse correlation for a particular sensor can rapidly be assessed. For large Doppler bandwidths and pulse periods measurements are independent. The reduction of either the pulse period or the Doppler bandwidth increases the level of measurement correlation, as evidenced by the HYDROS design.

The separation of \bar{V}_{kl}^a into three terms provides insight into causes of measurement covariance. For high chirp rates, the radar ambiguity function shows that separation of pulses in frequency has little effect, while separation of pulses in range rapidly decreases pulse-to-pulse covariance. Moreover, the cross-pulse gain product shows that covariance is minimized by spatially separating the pulses. Finally, the covariance phase expression shows that covariance is further minimized by using long pulse periods and large Doppler bandwidths. These three terms illustrate the tradeoffs involved between instrument design parameters and measurement covariance. Traditional instruments claim independence by virtue of $Q(x, y)$. New designs that overlap samples have large $Q(x, y)$ (near unity) and are, hence, dependent upon control of $B_{kl}(f_\omega)$ to minimize measurement covariance.

B. Range Resolution (\bar{V}^f)

Similar analysis can be used to evaluate the covariance expression for range filtered measurements, \bar{V}^f . While the processing is slightly different, the results of measurement correlation are similar. One key issue is the orientation of measurements as the antenna rotates about nadir. Antenna resolution measurements experience only fractional variations in Doppler bandwidth as a function of azimuth. Conversely, the Doppler bandwidth varies significantly with azimuth angle when using range-resolved measurements. Fig. 6 illustrates this phenomenon for three different azimuth angles. At 90° azimuth the bandwidth of each range measurement is equivalent to that of the footprint; at 0° , the Doppler bandwidth is minimal. The rotation of range-resolved measurements affects the behavior of $B_{kl}(k)$ with the decreased bandwidth of forward looking azimuths causing the sinc function to expand, increasing measurement correlation length.

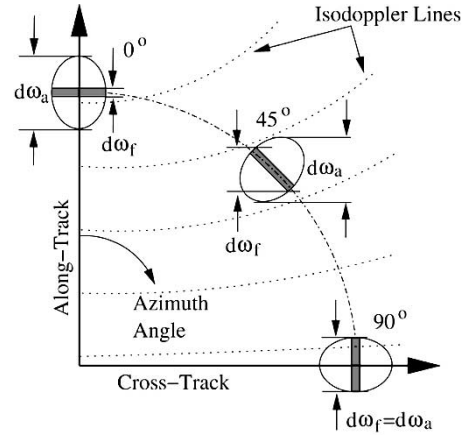


Fig. 6. Illustration of the effect antenna rotation has on the Doppler bandwidth of antenna footprint and range-resolved measurements. At 0° , the bandwidth of an antenna footprint ($d\omega_a$) measurement is maximum, and a range-resolved ($d\omega_f$) measurement is minimal. At 90° , the bandwidth of both measurements are equal.

V. MULTIPLE PULSE MEASUREMENTS AND THE EFFECTS OF CORRELATION

The accuracy of scatterometer measurements is commonly described by the normalized standard deviation of the measurement, termed K_p [6]

$$K_p = \frac{\sqrt{\text{Var}[\sigma_{\text{meas}}^o]}}{\sigma^o} = \sqrt{\frac{\text{Var}[M^u]}{(X\sigma^o)^2}}. \quad (53)$$

As part of the analysis, we consider the statistics of multiple pulse measurements. These measurements sum pulses either incoherently or coherently. Incoherent measurements are made by summing the squared response of each individual pulse in the measurements. Coherent processing is performed by combining pulses before the squaring operation, similar to synthetic aperture radar (SAR) processing. To determine the statistics of multiple pulse measurements we evaluate K_p to account for this processing.

A. Incoherent Measurements

To evaluate K_p for an incoherent multiple pulse measurement we define M^m as the mean of N_p single M^u measurements, processed using either footprint (12) or range filtering resolution (14)

$$M^m = \frac{1}{N_p} \sum_{k=1}^{N_p} M_k^u = \frac{1}{N_p} \sum_{k=1}^{N_p} \alpha M_k^{\text{sn}} + \beta M_k^n. \quad (54)$$

The expected value is then

$$\mathcal{E}[M^m] = \mathcal{E}[M^u] = X\sigma^o. \quad (55)$$

Using (46), the variance of M^m is

$$\text{Var}[M^m] = \mathcal{E}[(M^m)^2] - \mathcal{E}^2[M^m] \quad (56)$$

$$= \frac{1}{N_p^2} \sum_{l=1}^{N_p} \sum_{k=1}^{N_p} \text{Cov}[M_k^u M_l^u] \quad (57)$$

$$= \frac{1}{N_p^2} \sum_{l=1}^{N_p} \sum_{k=1}^{N_p} \mathbf{K}_{kl} \quad (58)$$

where \mathbf{K} is a covariance matrix with $\text{Cov}[M_k^u M_l^u]$ at the (k, l) th entry. If all of the pulses are independent, then \mathbf{K} is a diagonal matrix with zero entries for all off-diagonal elements. If the N_p pulses have some degree of correlation, \mathbf{K} is still diagonally symmetric, but off-diagonal terms may be nonzero. It can be shown that the correlation of two incoherent multipulse measurements is

$$\mathcal{E}[M_k^m M_l^m] = \frac{1}{N_p^2} \sum_{k=k_a}^{k_b} \sum_{l=l_a}^{l_b} \mathbf{R} + \mathbf{K} \quad (59)$$

where $(X_k X_l / \bar{R}_k \bar{R}_l)(R_k R_l)$ is the (k, l) th entry of \mathbf{R} , and that the covariance of two measurements is

$$\text{Cov}[M_k^m M_l^m] = \frac{1}{N_p^2} \sum_{k=k_a}^{k_b} \sum_{l=l_a}^{l_b} \mathbf{K}. \quad (60)$$

According to (46) and (49), it is possible that some of the off-diagonal elements of \mathbf{K} are negative, though the matrix is positive semidefinite. This suggests that it is possible to reduce the overall variance of multiple pulse measurements by sampling at an appropriate interval, allowing negative values in \mathbf{K} to offset positive values. This ability to minimize measurement variance through negatively correlated pulses is limited to instruments with short pulse periods (T_p) and small N_p as dictated by $B_{kl}(k)$.

Next we explore the behavior of \mathbf{K} relative to key instrument parameters. First, let $K_p(N_p)$ be

$$K_p(N_p) = \sqrt{\frac{\sum_{l=1}^{N_p} \sum_{k=1}^{N_p} \mathbf{K}_{kl}}{N_p^2 \mathbf{m}^T \mathbf{m}}} \quad (61)$$

with

$$\mathbf{m} = \frac{1}{N_p} [X\sigma_1^o, X\sigma_2^o, \dots, X\sigma_{N_p}^o]^T. \quad (62)$$

This allows determination of the effectiveness of multiple pulse measurements using

$$J_{K_p}(N_p) = \frac{K_p(N_p)}{K_p(1)} \quad (63)$$

the ratio of the multimeasurement K_p normalized by the single measurement K_p . In doing so, we assume that the means of the measurements are statistically identical. In general, the tradeoff for using N_p pulses is reduced spatial resolution. Oversampling seeks to reduce K_p using large N_p without significantly degrading resolution. It can be seen that if the N_p pulses are all independent, $J_{K_p}(N_p)$ is $1/\sqrt{N_p}$. Likewise, if the pulses are completely dependent (i.e., identical), \mathbf{K} is a matrix with equal elements and $J_{K_p}(N_p) = 1$.

Furthermore, K_p is a function of the SNR. The multiple pulse covariance matrix can be expressed as

$$\mathbf{K} = \mathbf{K}_V + s\mathbf{I} \quad (64)$$

where \mathbf{K}_V is the contribution to \mathbf{K} from the random fading in the signal, \mathbf{I} is an identity matrix, and the scalar s represents the contribution from additive noise [see (43)]

$$s = \frac{2RN_s}{X} + \frac{4N_s^2}{X^2}. \quad (65)$$

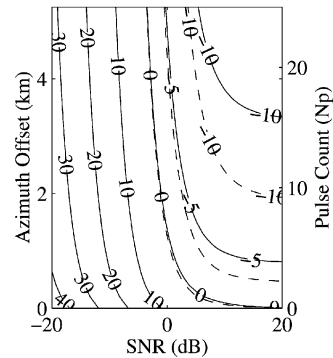


Fig. 7. Contour plot of normalized variance (K_p^2) as a function of SNR and azimuth offset and pulse count in decibels ($20 \log_{10} K_p$) for HYDROS at 90° azimuth angle. The right axis is the number of pulses included in the variance sum (58), while the left axis is the corresponding azimuth distance (in km). The solid lines represent the variance for HYDROS pulses, the dashed lines represent measurement variance if the pulses were independent.

For high SNR, s is small and $\mathbf{K} \approx \mathbf{K}_V$. For low SNR, s is large and $\mathbf{K} \approx s\mathbf{I}$, reducing covariance but not necessarily improving K_p . This introduces the tradeoff between the correlation of the pulses and the operating SNR.

Fig. 7 illustrates the tradeoff between multiple pulses, measurement correlation and SNR for HYDROS. The data is derived from Fig. 5, the 90° azimuth calculation of signal covariance. The figure plots normalized measurement variance as a function of azimuth offset (pulse count) and SNR. The figure shows that combining several pulses improves K_p , particularly at high SNR. It also shows that for large N_p a proportionally greater benefit can be derived from improving SNR rather than increasing N_p . Finally, it shows that small SNR changes have little effect on measurement correlation. While the results of this plot are specific to instrument geometry and waveform, general insight is gained by noting that pulse-to-pulse covariance primarily effects measurements with high SNRs and large pulse counts.

B. Coherent Measurements

The other option in multiple pulse measurement is coherent combination. The disadvantage of this approach is the significant increase in signal processing complexity. The advantages of this SAR-like processing is the improvement in signal variance and resolution by range and frequency filtering [3]. While significantly more complicated to implement, coherent processing allows for extraction of the maximum number of independent samples from the measurement that can be used to provide maximum resolution or be averaged to minimize the measurement K_p . The variance of incoherent measurements is proportional to $1/N_p$, while the variance of coherent processing is proportional to $1/N_p^2$ [4].

VI. SUMMARY

General expressions for correlation and covariance between pulses have been derived for scatterometer measurements. These expressions can be adapted to specific instruments. Expressions for several different types of measurements for signal-only, signal-plus-noise, and noise-only have been shown. A numerical evaluation of the signal covariance has

been presented for two scatterometer designs, showing basic behavior of correlation and covariance between pulses as a function of pulse offset, pulse width, and Doppler bandwidth. The effects of correlation on signal variance and K_p have been demonstrated for the incoherent case. It was shown that \bar{K}_p for multiple pulses is always less than or equal to K_p for a single pulse measurement. It is concluded that correlation between measurements for high PRF instruments must be considered in the design process. Correlation can be minimized through proper selection of pulse rates and measurement dimensions. Measurement variance can be improved and correlation reduced by combining multiple pulses, both incoherently and coherently to make single backscatter measurements of the surface.

REFERENCES

- [1] M. R. Drinkwater and C. C. Ling, "Introduction to the special section on emerging scatterometer applications," *IEEE Trans. Geosci. Remote Sensing*, vol. 38, pp. 1763–1764, July 2000.
- [2] D. S. Early and D. G. Long, "Image reconstruction and enhanced resolution imaging from irregular sampling," *IEEE Trans. Geosci. Remote Sensing*, vol. 39, pp. 291–302, Feb. 2001.
- [3] M. W. Spencer, W. Y. Tsai, and D. G. Long, "High-resolution measurements with a spaceborne pencil-beam scatterometer using combined range/doppler discrimination techniques," *IEEE Trans. Geosci. Remote Sensing*, vol. 41, pp. 567–581, Mar. 2003.
- [4] F. Ulaby, R. Moore, and A. Fung, *Microwave Remote Sensing: Active and Passive*. Norwood, MA: Artech House, 1986, vol. 2.
- [5] D. G. Long and M. W. Spencer, "Radar backscatter measurement accuracy for a spaceborne pencil-beam wind scatterometer with transmit modulation," *IEEE Trans. Geosci. Remote Sensing*, vol. 35, pp. 102–114, Jan. 1997.
- [6] R. Fisher, "Standard deviation of scatterometer measurements from space," *IEEE Trans. Geosci. Electron.*, vol. GE-10, Apr. 1972.
- [7] M. W. Spencer, C. Wu, and D. G. Long, "Improved resolution backscatter measurements with the SeaWinds pencil-beam scatterometer," *IEEE Trans. Geosci. Remote Sensing*, vol. 38, pp. 89–104, Jan. 2000.
- [8] F. Ulaby, R. Moore, and A. Fung, *Microwave Remote Sensing: Active and Passive*. Norwood, MA: Artech House, 1986, vol. 1.
- [9] M. Spencer, private communication.

- [10] E. Njoku, Y. Kim, M. Spencer, W. Tsai, W. Wilson, S. Yueh, J. van Zyl, Y. Rahmat-Samii, and M. Thomson, "A spaceborne L-band radiometer-radar concept for land and ocean surface monitoring," in *Proc. IEEE Aerospace Conf.*, Big Sky, MT, Mar. 2001.



Peter K. Yoho (S'00–M'03) received the Ph.D. in electrical engineering from Brigham Young University, Provo, UT, in 2003.

He is currently with the Lincoln Laboratory, Massachusetts Institute of Technology, Lexington, MA, where his work concentrates on radar system design and clutter mitigation.



David G. Long (S'80–SM'98) received the Ph.D. degree in electrical engineering from the University of Southern California, Los Angeles, in 1989.

From 1983 to 1990, he was with the National Aeronautics and Space Administration (NASA) Jet Propulsion Laboratory (JPL), Pasadena, CA, where he developed advanced radar remote sensing systems. While at JPL, he was the Senior Project Engineer on the NASA Scatterometer (NSCAT) project, which was flown aboard the Japanese Advanced Earth Observing System (ADEOS) from 1996 to 1997. He was also the Experiment Manager and Project Engineer for the SCANSAT scatterometer (now known as SeaWinds). In 1990, he joined the faculty of the Electrical and Computer Engineering, Brigham Young University (BYU), Provo, UT, where he currently teaches upper division and graduate courses in communications, microwave remote sensing, radar, and signal processing, is the Director of BYU's Center for Remote Sensing, and is the Head of the Microwave Earth Remote Sensing Laboratory. He is the Principal Investigator on several NASA-sponsored interdisciplinary research projects in microwave remote sensing and innovative radar systems. He has numerous publications in signal processing and radar scatterometry. His research interests include microwave remote sensing, radar, polar ice, signal processing, estimation theory, and mesoscale atmospheric dynamics. He has over 250 publications in the open literature.

Dr. Long has received the NASA Certificate of Recognition several times.